Arch. Min. Sci. **71** (2026), 2, 269-291

Electronic version (in color) of this paper is available: http://mining.archives.pl

DOI: https://doi.org/10.24425/ams.2026.158817

PHU MINH VUONG NGUYEN[1], BARTOSZ APANOWICZ[1*],
ANDRZEJ WALENTEK[1], SHOUKAI CHEN[2], JINPING LIU[2]

PREDICTION OF SURFACE UPLIFT IN POST-MINING AREAS USING SATELLITE INTERFEROMETRY AND NUMERICAL MODELLING – A CASE STUDY

In most coal mines across Europe, mining operations have already ceased, and the previously exploited geological strata have become partially or fully flooded. The process of mine flooding is gradual, often spanning several years or even decades. During this time, the water table within the re-saturating rock mass slowly rises toward the surface. As groundwater infiltrates and saturates the rock, it induces geomechanical changes, including the movement of rock blocks within the geological strata and the redistribution of local gravitational stresses. These changes result in stress accumulation and alterations in the geodynamic equilibrium of the region. Ultimately, such processes can lead to large-scale ground movements, including land subsidence, uplift, or the sudden formation of sinkholes in near-surface areas. Understanding and monitoring these phenomena are critical for mitigating geohazards associated with post-mining environments and ensuring the long-term stability of former mining regions. To support this goal, a study was conducted to predict surface uplift at the flooded Kazimierz-Juliusz coal mine in Poland using numerical modelling with FLAC2D, a finite difference method-based software. Based on extensive Satellite Radar Interferometry (InSAR) monitoring data, a numerical model was developed and subsequently verified for predictive analysis. Occurrence of surface uplift has been observed at the studied site, with a maximum displacement of approximately 16 cm at the end of 2023. Long-term predictions indicate that surface uplift could reach up to 57 cm when the water level rises to ground level. This research is expected to provide a valuable reference for understanding uplift phenomena and to contribute to a deeper insight into water-mechanical interactions within the rock mass in regions affected by mine flooding.

Keywords: Surface uplift; mining-induced deformation; numerical modelling; InSAR; deformation prediction

[1] CENTRAL MINING INSTITUTE, PLAC GWARKÓW 1, 40-166 KATOWICE, POLAND
[2] NORTH CHINA UNIVERSITY OF WATER RESOURCES AND ELECTRIC POWER, CHINA

* Corresponding author: bapanowicz@gig.eu

1. Introduction

Surface deformation is a well-documented phenomenon in mining regions and can manifest in various forms, including both subsidence and uplift. The characteristics of surface deformation are influenced by a wide range of parameters, such as the number and thickness of the mined coal seams, the depth and inclination of these seams, surface topography, the lithological composition of the overburden, and the presence of geological structures such as faults and water-bearing formations [1-7].

Typically, subsidence tends to occur during active mining operations and can continue for many decades following mine closure. However, in some post-mining environments, particularly those undergoing mine flooding, the rebound of underground water levels plays a critical role in inducing ground uplift rather than subsidence [8-14]. As the groundwater table gradually rises, the resulting increase in pore pressure within the rock mass leads to stress redistribution and may induce volumetric expansion in certain geological strata. Additionally, the mechanical behaviour of unconsolidated deposits - such as caved zone (goafs) and fracture zone - can further influence surface deformation, as these zones may undergo compaction or swelling in response to changes in water content.

An example of such uplift is currently being observed at the abandoned "Kazimierz-Juliusz" coal mine in Poland, which was fully decommissioned by the end of 2018. Since closure, the ground surface has risen by approximately 15 cm, accompanied by a consistent and measurable increase in the underground water level. This scenario illustrates the complex interaction between hydrogeological and geomechanical processes in post-mining settings, making the prediction of surface uplift particularly challenging.

To address this issue, the relationship between surface deformation and the rising groundwater table was systematically investigated. The primary objective of the study was to establish approximate correlation estimates that could aid in characterising and forecasting the evolution of surface uplift in response to continuous groundwater recovery. For this purpose, an integrated analysis was performed, combining numerical modelling techniques with Satellite Radar Interferometry (InSAR) monitoring data. This hybrid approach enables the identification of spatial and temporal patterns in surface displacement and their potential linkage to subsurface hydrodynamic changes. By examining these correlations, the study aims to enhance the understanding of hydrogeomechanical behaviour in flooded mining regions and improve predictive capabilities for managing surface impacts. The findings contribute to a growing body of knowledge essential for mitigating risks associated with ground deformation in post-mining environments and for guiding future land-use planning in affected areas.

2. Overview of prediction methods for mining-induced deformation of the ground surface

Depending on the available information about the geomechanical properties of the rock mass and the geological and mining conditions, methods for predicting mining-induced deformations can be divided into two major approaches: empirical methods and numerical methods [4]. The first group, empirical methods, belongs to the category of parametric methods. These methods use the influence function or the profile function of the subsidence basin to describe the impact of mining deformations on the surface of the terrain, i.e., the interaction of mining activities [15,16]. The first theory using the influence function was the Keinhorst theory [17], later developed by Bals [18]. The assumption of the theory was to limit the area of influence. Other examples include the widely used Knothe method [19,20] in Poland and the Ruhrkohle method [21] used in Germany. Mathematically, these methods are identical, with the only difference being in the definition of the angle of influence. An example of a model using the interaction function of mining activities is the Sroka method [22], which allows for the consideration of changing boundary conditions. These kinds of methods are based on calibrating the model using geodetic data. Empirical relationships are derived to predict mining deformations [23-26].

Numerical methods offer advanced tools for analysing engineering problems, allowing for the consideration of complex geometries, influencing factors, and various mechanisms that are unattainable using empirical or analytical methods. Additionally, the rapid development of computer technologies over the last decade has led to an increasing use of numerical methods in geoengineering analyses, such as assessing and/or predicting surface deformations. Before applying numerical calculations to solve geoengineering problems, an appropriate material model must be selected, i.e. suitable properties must be assigned to the rock mass. The rock mass can be assumed as an elastic medium, a transversely isotropic elastic medium, an elastoplastic medium or others. Many numerical methods were applied to study surface deformation with different effects that reflect the measured surface displacements. Yao et al. [27] presented a non-linear finite element package, and its modifications allow modelling of the ground movement due to mining inclined seams. The results have been validated by comparison with both empirical models and physical modelling results. This study focused on the effect of dip of the mineral seam and the width/depth ratio on subsidence, displacement, stress and strain distribution. Keilich [28] introduced a methodology of subsidence prediction using the distinct element method-based code as an alternative for modelling and prediction of subsidence induced by isolated longwall panels. The numerical models have been validated by comparison with empirical results, observed caving behaviour and analytical solutions. Sayyaf et al. [29] used 2D finite element method to simulate the land subsidence induced by the excessive use of groundwater resources in Kerman province, Iran. Suchowerska Iwanec et al. [30] compared predictions of surface subsidence obtained using the finite element method, considering a range of well-known constitutive models. Based on the field measurements of surface subsidence, the advantages and disadvantages of each selected constitutive model are discussed. Huang et al. [31] studied subsidence due to ore extraction and backfilling during open stoping operations at an underground iron mine in China. A 3-D distinct element discontinuum numerical model was performed, incorporating geologic complexities including faults and interfaces between different lithologies, and the stopping and backfilling sequence adopted from the mine plans. Das et al. [32] analysed the pattern of surface settlement due to non-circular asymmetric parallel tunnel deformation under natural undulating topography using a finite element method-based code. A transportation tunnel project in the Bilaspur district of Himachal Pradesh, India has been taken as an example. Hamdi et al. [33] presented a finite/discrete element modelling approach coupled with a discrete fracture network (FDEM-DFN) to analyse the Kiruna (Sweden) hanging wall surface subsidence with an emphasis on investigating the influence of discontinuity persistence and spacing. Cao et al. [34] introduced a simulation of the surface subsidence induced by a mining method called ”wide strip backfill mining” using three-dimensional finite difference numerical simulation. The case study took place at Taoyi coal mine located in the Handan mining area, Hebei Province, China. Voyiadjis and Zhou [35] introduced an analysis of surface subsidence of the Valentine gas field in coastal

Louisiana during and after production using three-dimensional finite element modelling. Li et al. [36] presented a two-dimensional numerical model, established by the discrete element method code PFC2D, to investigate the mechanical mechanism of surface subsidence and backfill material movement induced by underground mining in the Hongling lead-zinc mine located in northern China. Zhao et al. [12] describe a case study of surface subsidence in the Hongling Lead-Zinc Mine located in Inner Mongolia, China. A three-dimensional finite-difference numerical simulation was carried out to analyse the excavation procedure and mechanism. The results of the simulation were in good agreement with the field subsidence data collected by satellites and aerial vehicles. Shi et al. [37] combined three-dimensional finite-difference numerical simulation and probabilistic integral method to predict surface deformation due to the extraction of underground coal in the Jindal Coal mine located in Tengzhou city, Shandong province, China. Zhao et al. [38] introduced a three-dimensional finite difference numerical model of the Jinfeng Gold Mine in Guizhou Province, China, to estimate the shaft stability and surface deformation induced by underground mining transferred from open-pit mining. Satellite monitoring data of surface displacement at several points were used to calibrate the numerical model. Guo et al. [39] studied the surface movement and deformation law of deep continuous mining by caving method in the Shizishan mining area, Yunnan Province, China, integrating the field fissures investigation, GPS monitoring, and large-scale three-dimensional finite-difference numerical simulation. Li et al. [40] introduced an in-depth investigation of surface subsidence using the three-dimensional finite-difference numerical simulation. The research focuses on the Prang Copper Mine subsidence area in Yunnan Province, China. The uneven surface subsidence induced by underground structural interfaces and underground mining activities was modelled. For the conditions of Polish coal mining, numerical methods for predicting surface deformations have been applied by many researchers, e.g. Kwaśniewski and Wang [41], Florkowska [42], Tajduś [43-46], Wesołowski [47,48], Dudek [11,49,50]. These studies were conducted using the finite element method (FEM) with an appropriate selection of transversely isotropic model properties. The outcomes showed high agreement with those calculated using Knothe's theory and in situ surface displacement measurements.

The issue of ground surface uplift induced by mine closure and/or flooding of old underground workings is relatively uncommon, with a limited number of reported case studies. This is mainly because large-scale mine closures only began in the last decade, and the uplift process requires sufficient time to fully develop and become clearly observable. According to Zhao et al. [51], the first applications of numerical tools for simulating uplift have appeared since 2019. Todd et al. [52] developed a 2D coupled hydromechanical model to simulate the uplift of abandoned, flooded mine workings in Scotland. Dudek and Tajduś [49] stated that predicting surface uplift induced by mine flooding is possible using numerical methods. In their research, a series of numerical calculations was performed using the FEM, representing steeply inclined seams based on the authors' methodology [11]. The surface deformation results were presented and verified by measurements. Zhao and Konietzky [53] proposed a numerical modelling strategy that includes three phases: the initial state before mining, the stage directly after mine closure, and the flooding stage. In situ measurements are used to calibrate the model. The case study was conducted at the Oelsnitz abandoned coal mine, where the data were used for model validation and prediction. At the same time, predictive approaches based directly on InSAR time series are being developed. These include point-based modelling of uplift evolution using the cumulative distribution function (CDF) of the Weibull distribution. This approach offers a new trend in surface uplift prediction without requiring in situ geological and hydrological data from the studied sites [54].

Currently, a common approach to predicting surface deformation is coupling numerical analysis with the results of laboratory and in-situ tests, as well as in-situ measurements (monitoring). In this study, the extensive data obtained from monitoring of surface deformation using satellite interferometry and the two-dimensional finite-difference numerical simulation are used to predict the surface uplift at a liquidated underground mine located in Poland.

3. Case study – the liquidated "Kazimierz-Juliusz" coal mine

3.1. Location and general information

The "Kazimierz-Juliusz" hard coal mine is located in the northeastern part of the Upper Silesian Coal Basin (USCP), Poland. The mining area of the mine covers 23.08 km^2 and is located mainly within the administrative boundaries of the Sosnowiec city, with parts extending into the cities of Jaworzno and Dabrowa Górnicza. The mine began operations in the 19th century with open-pit mining, and at the turn of the 19th and 20th centuries, underground coal extraction started, continuing for over 100 years. In May 2015, the mine was officially decommissioned. In 2016, the flooding of underground workings began, and the mining plant was completely liquidated by the end of 2018. Currently, the mine is completely abandoned. The location of the mine is shown in Fig. 1.

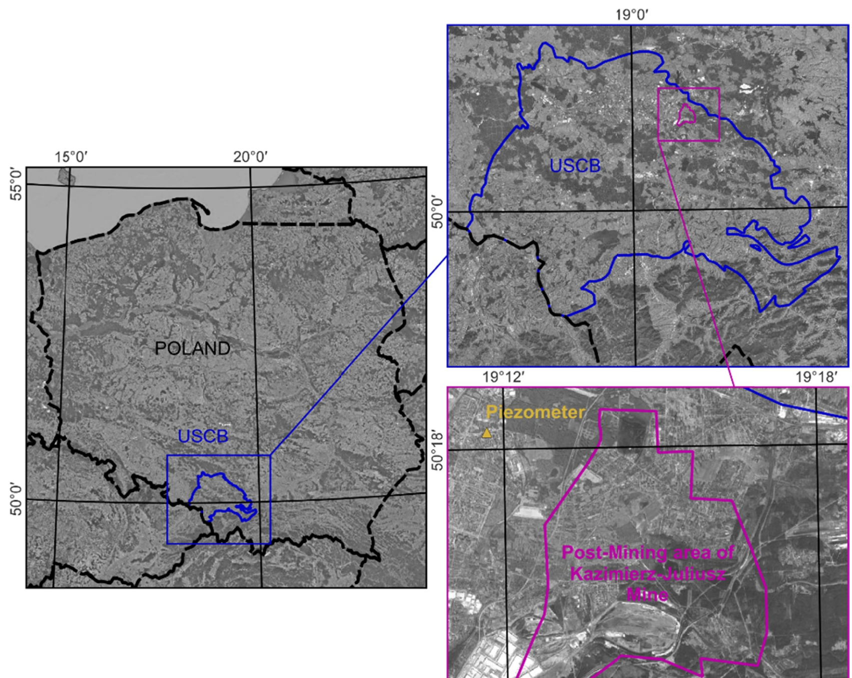

Fig. 1. Location of the "Kazimierz-Juliusz" coal mine with the location of the piezometer

Coal mining within the analysed post-mining area was conducted in nine coal seams. In the western part, extraction took place in seams No. 409/1-2, 418, and 420, belonging to the Ruda and Saddle layers, at depths reaching up to 740 m. Their thickness ranged from 1.2 meters to several meters. In the northeastern part, mining was carried out in the marginal layers, including seams No. 816, 819, 823, 829, and 833, with thicknesses ranging from 1.2 to 2.4 meters. Additionally, extraction from seam No. 510 was conducted across the entire area, with thickness varying between 3 and 10 meters (TABLE 1). A detailed description of the mining operations carried out in the analysed post-mining area, along with a map showing the contours of this exploitation, is presented in [55].

TABLE 1

Summary of information on the mining operations carried out at the "Kazimierz-Juliusz" coal mine

Seams	Layers	Depth [m]	Thickness [m]	Location
409/1-2	Ruda and Saddle	up to 700	1,2 – several meters	Western part of mining area
418				
420				
816	Marginal	up to 420	1,2 – 2,4	North-eastern part of mining area
819				
823				
829				
833				
510	Sandstones and Claystones	up to 700	3 – 10	Across entire area

3.2. Brief characteristics of geological and hydrogeological conditions at the studied site

In the geological structure up to a depth of approximately 800 m, two main formations are present. The Quaternary formations extend down to 6.5 m and consist of embankment material-rubble, slag, sand, and clay. Beneath them, the Carboniferous formations contain layers of clay shales, sandy shales, and sandstones, along with coal seams. The average dip of the Carboniferous layers is approximately 22 degrees. Fig. 2 shows an example of geological structure in the studied site along the ventilation shaft. No major tectonic disturbances are observed at this specific location. However, the general tectonic structure of the study area is highly varied, with fault displacements reaching up to 200 m [55]. A water-bearing level is present in the Quaternary sands at a depth of approximately 7 m. Additionally, several Carboniferous water-bearing levels have been identified: the first at a depth of 92-102 m, the second at 160-190 m, the third at 260-270 m, and the fourth at 300-360 m.

Groundwater monitoring in the post-mining area of the "Kazimierz-Juliusz" mine is conducted using piezometers of varying depths. The study used data from a piezometer borehole monitoring deep Carboniferous aquifers, which is located about 2.2 km northwest of the analysed area (piezometer coordinates: 50.3036N, 19.1946E). Currently, there is no piezometer within the analysed area monitoring the level of Carboniferous groundwater. Recorded water level changes in time function are shown in Fig. 3. The monitoring period covered from July 2021 to February 2023.

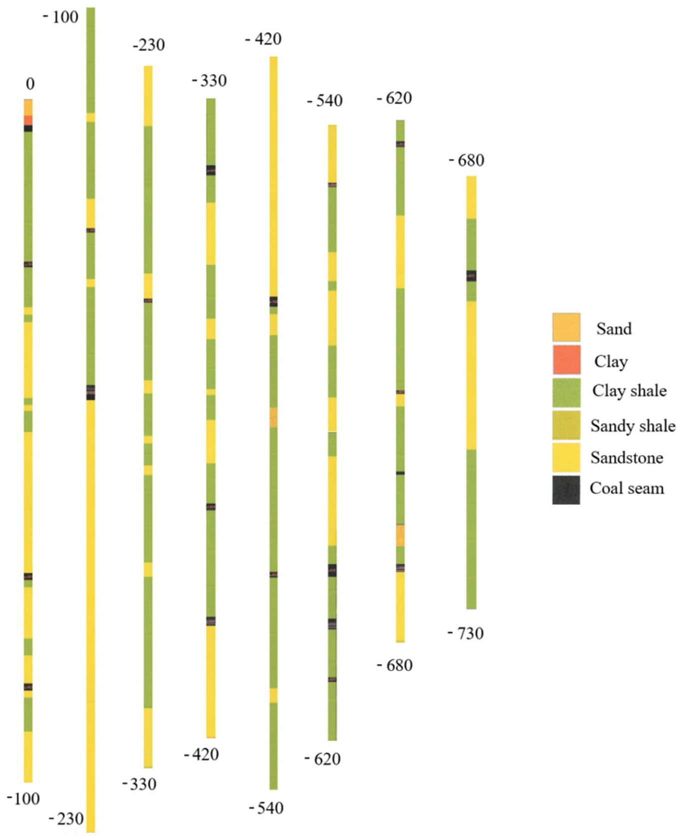

Fig. 2. Geological profile along the ventilation shaft of the "Kazimierz-Juliusz" Coal Mine

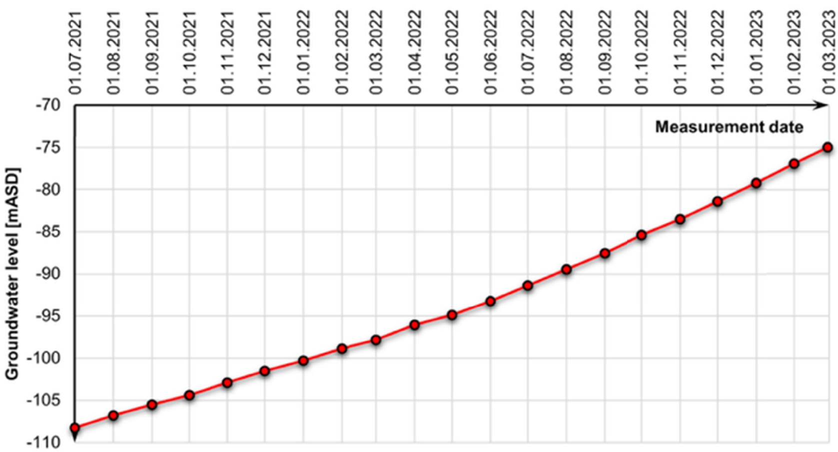

Fig. 3. Change in the level of Carboniferous groundwater recorded by a piezometer between July 2021 and February 2023

As shown in Fig. 3, the groundwater level systematically increased from –108.251 mASD to –74.979 mASD between July 2021 and February 2023. The total rise during the analysed period was 33.272 m, progressing at an average rate of approximately 1.7 m per month. The above data were collected and provided as part of the PostMinQuake RFCS Research Project for the field site in Poland [56].

4. Monitoring of Surface deformation using Satellite Interferometry Radar (InSAR)

4.1. General background and applications

Satellite radar interferometry (InSAR) is an advanced remote sensing technique that uses synthetic aperture radars (SAR) mounted on satellites orbiting the Earth in Low Earth Orbit (LEO). The principle of SAR operation is based on sampling the Earth's surface from different satellite positions and at various angles. Then, the signal is combined into a complete image. This approach allows for high resolution (from a few to several meters) with relatively small antenna sizes (up to a few meters). SAR radars are active sensors, which enable operation regardless of the time of day or weather conditions [57,58]. The concept of InSAR is based on analysing phase differences of radar signals reflected from the same part of the Earth's surface at different times or from different satellite positions. This involves calculating the difference between two SAR images, which are measurement products containing information about a complex number consisting of the signal phase (φ) and signal amplitude (j) [59]. The result of this difference is an interferogram – a matrix containing the phase shift between two SAR images, known as the interferometric phase (1) [60]:

$$\Delta\varphi = \frac{4\pi}{\lambda} \times \Delta r \tag{1}$$

where: λ is the radar wavelength; Δr is the difference in distance between the Earth's surface and one of the other satellites, or the same satellite at different times. If there is no surface displacement, the interferometric phase can be used to determine the topography of the Earth's surface by considering precise orbital parameters. If surface displacements occur between two SAR acquisitions, the interferometric phase contains information about both the terrain topography and the surface deformations that have taken place (2) [60]:

$$\Delta\varphi = \Delta\varphi_{topo} + \Delta\varphi_{defo} \tag{2}$$

where: $\Delta\varphi_{topo}$ is the interferometric phase component related to terrain topography; $\Delta\varphi_{defo}$ is the interferometric phase component related to surface displacement. To determine surface displacements, it is necessary to separate and remove the topographic component. In practice, InSAR measurements are affected by various factors, such as system errors, orbital uncertainties, atmospheric delays, and phase noise, all of which must be considered when calculating surface displacements. Additionally, the radar signal is modulated within a 2π range, meaning that the unwrapped phase must also be retrieved [61-63]. This approach is known as differential interferometry (DInSAR) [64].

An extension of the classical DInSAR method includes advanced time series algorithms (MT-InSAR), such as the permanent scatterers method (PSInSAR) [65,66] and the small baseline subset method (SBAS) [67]. The PSInSAR method is based on processing a set of SAR images, where one serves as a reference image and multiple others as secondary images. Interferograms are calculated between the reference image and the secondary images. Calculations are performed for permanent scatterer points (*PS*) where the radar signal reflection remains stable. *PS* points can be selected in different ways, but the two most common methods are selection based on amplitude dispersion [66] or on the temporal coherence of a given pixel [68]. The interferometric phase for a *PS* point is given by (3) [65,68]:

$$\Delta\varphi_{PS} = \frac{4\pi}{\lambda}\left(d + B_{\perp} \times \Delta z\right) + \Delta\varphi_{atm} + \Delta\varphi_{noise} \tag{3}$$

where: d is the actual surface displacement in the satellite's line of sight (LOS); $B_{\perp}$ is the baseline; $\Delta\varphi_{atm}$ is the interferometric phase component related to atmospheric delays; $\Delta\varphi_{noise}$ is the interferometric phase component related to phase noise. The SBAS method is based on processing a set of SAR images, where multiple reference and secondary images are used. Interferogram pairs are selected based on spatial and temporal baselines. Minimising these baselines helps reduce orbital errors affecting the interferometric phase and decreases signal decorrelation caused by surface changes between two SAR acquisitions. The interferometric phase in the SBAS method is given by (4) [67]:

$$\begin{aligned}\Delta\varphi(r,A) &= \varphi(t_B,r,A) - \varphi(t_A,r,A) \\ &\approx \frac{4\pi}{\lambda}\left[d(t_B,r,A) - d(t_A,r,A)\right] + \frac{4\pi}{\lambda} \times \frac{B_n \Delta z}{r \sin\theta} \\ &+ \left[\varphi_{atm}(t_B,r,A) - \varphi_{atm}(t_A,r,A)\right] + \Delta n \end{aligned} \tag{4}$$

where: r, A are the coordinates of a given pixel in range (r) and azimuth (A); t_B, t_A are the acquisition times of the given image; φ is the phase signal value; d is the cumulative displacement in the satellite's line of sight (LOS); Δz is the terrain topography error; *atm* is the phase component determined by atmospheric delays; Δn is the phase component determined by phase noise. The analysis of a large number of SAR images in MT-InSAR methods allows for the estimation and subsequent separation of patterns related to atmospheric delays affecting the signal. Additionally, there are less commonly used satellite image processing methods that build upon the previously described techniques, such as the multi-view method [68], the MSBAS (Multidimensional Small Baseline Subset) method [8], or the MAI (Multiple Aperture Interferometry) method [70].

InSAR methods have been widely used for monitoring surface displacements related to natural processes [71], glacier movements [72], deformations caused by volcanic eruptions [73], and earthquakes [74]. Regarding mining areas, InSAR has been applied in Australia [75], China [76], and Europe [77]. In post-mining regions, it has also been extensively used to identify residual deformations and surface uplift caused by the flooding of abandoned mining excavations [8,9,78,81].

4.2. Applications of satellite interferometry for the studied site

Long-term surface displacements in the study area were determined using SAR images acquired at 6-day and 12-day time intervals by the Sentinel-1 satellite constellation. The images were processed using the SBAS method, as two time series from two satellite pass orbits: ascending orbit number 175 and descending orbit number 51. Interferograms were calculated through a two-pass processing using GMTSAR software [82], and the interferometric phase was unwrapped using a two-way phase unwrapping method implemented in the SNAPHU application [63]. The topographic and atmospheric phase components were removed using SRTM-1 data [83] and GACOS corrections [84-86], respectively. Additionally, to reduce imperfections such as noise, the unwrapped phase was further filtered by fitting the results to a low-order polynomial trend using the least squares method and removing mismatched imperfections. For this purpose, an algorithm implemented in GMT software was used [87]. The result of the computational process was two sets of time series containing information about the cumulative surface displacements in the LOS direction. The analysis of two independent data sets allowed for the decomposition of the two LOS vectors to distribute surface displacements into vertical and horizontal displacements in the east-west direction [59].

The time analysis covered the period from the beginning of 2015 to the end of 2023. The number of processed interferograms was 2985 for orbit number 175 and 2733 for orbit number 51. Detailed information about the computational parameters is summarised in TABLE 2.

TABLE 2

Basic information on the SAR data and SBAS time series processing and results used in the studies

Calculation period	**January 2015 – December 2023**	
Sensor	Sentinel-1A/B	
Orbit number/IW	175 / IW2-IW3	51 / IW2-IW3
Orbit type	Ascending	Descending
Number of SAR images in time series	426	406
Perpendicular baseline [m]	120	120
Temporal baseline [days]	60	60
Number of interferograms	2985	2733

4.3. Monitoring results analysis

The analysis of the obtained results revealed the occurrence of surface uplift across the entire post-mining area of the Kazimierz-Juliusz mine. Only two areas, located in the southeastern and southwestern parts of the site, did not experience uplift. The largest uplift basin, measuring approximately 2.5 km in the N-S and W-E directions, formed in the central-western part of the area. The highest cumulative surface uplift in this region, recorded between January 2015 and December 2023, reached up to 16 cm (Fig. 4).

Changes in ground surface topography in time function, in six-month intervals, are presented in two graphs along the designated N-S and W-E profiles, located in the area of the highest surface uplifts (Figs. 5 and 6). Additionally, Fig. 7 shows the increase in ground surface uplift in time function at the location of the largest uplifts, that is, at 780 m of the W-E profile. According to the graphs, the maximum surface uplift reached over 17 cm in the first half of 2023. Subsequently, over the next six months by the end of 2023, the ground surface subsided by approximately 1 cm at this location. The most significant uplift increase occurred between January 2021 and July 2021, reaching 33 mm at 960 m of the N-S profile and 30 mm at 1800 m of the W-E profile. This was

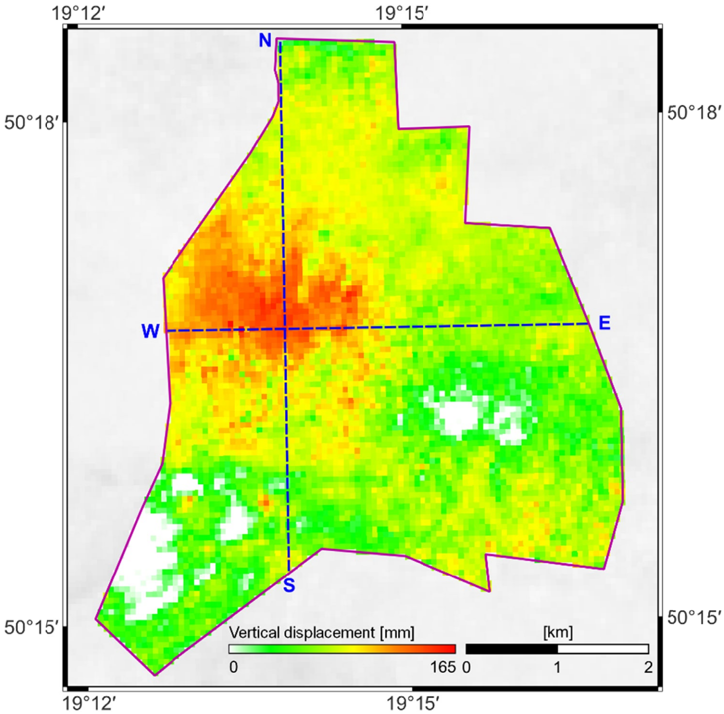

Fig. 4. Cumulative vertical surface displacements in the post-mining area of "Kazimierz-Juliusz" (January 2015 – December 2023), obtained from SAR image processing using the SBAS method, along with the location of N-S and W-E profiles (blue line)

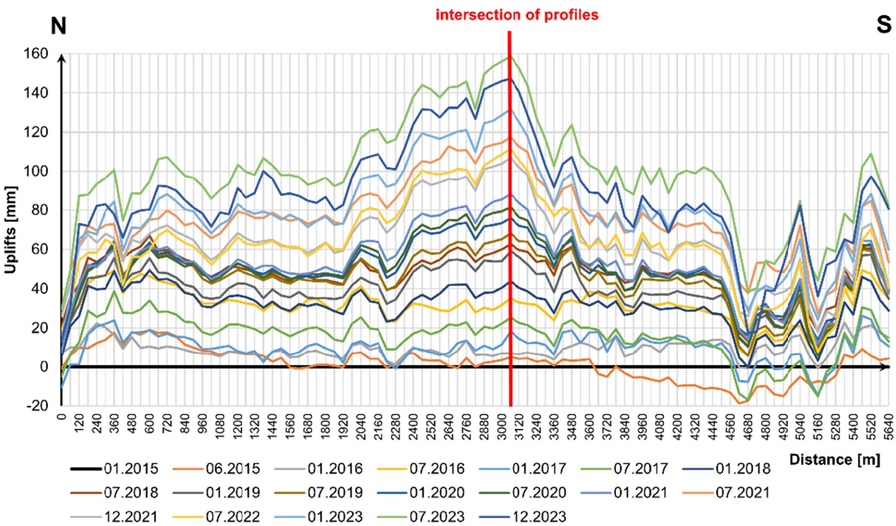

Fig. 5. Vertical ground surface uplifts along the N-S profile obtained from SAR image processing using the SBAS method

followed by a surface subsidence of several millimetres and stabilisation until January 2022 and July 2022, respectively. Later, until July 2023, another significant uplift increase was observed, reaching approximately 48 mm at 1260 m of the N-S profile and 50 mm at 780 m of the W-E profile. Finally, according to the obtained results, the surface of the analysed area uplifted at the highest average rate of 19 mm/year.

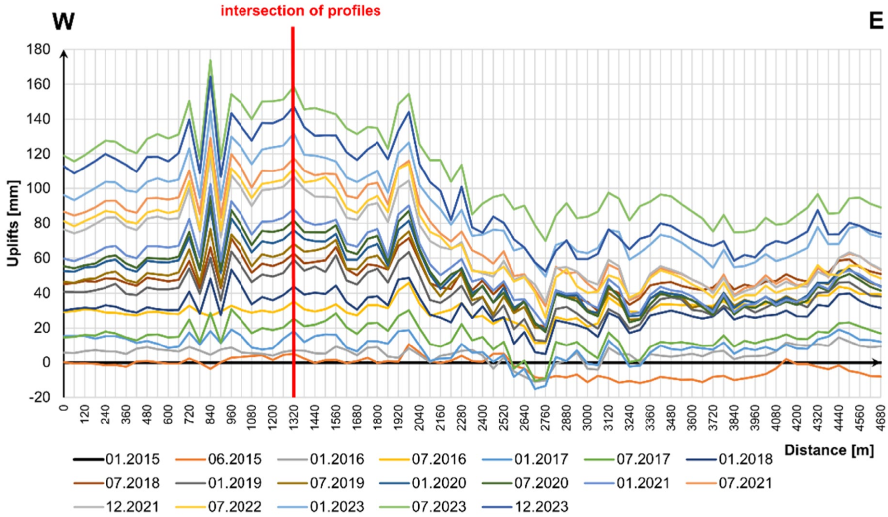

Fig. 6. Vertical ground surface uplifts along the W-E profile obtained from SAR image processing using the SBAS method

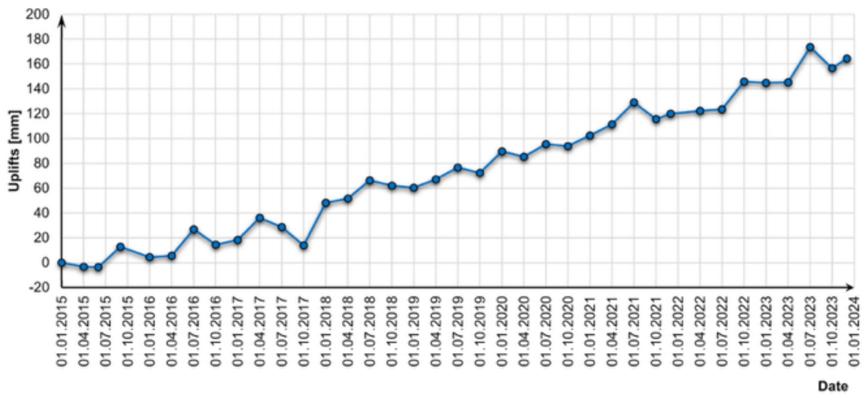

Fig. 7. Vertical ground surface uplifts in time function at 780 m of the W-E profile obtained from SAR image processing using the SBAS method

Fig. 8 presents the change in surface uplift due to the rise in the underground water level. The groundwater levels increased by approximately 33 m, while the ground surface rose by about 50 mm. It can be noticed that the increase in water levels was generally proportional to the ground surface uplift. The coefficient of determination for both variables was 0.6027, which means that the Pearson correlation coefficient is 0.7763. Therefore, it can be stated that the two variables, surface uplift and groundwater level rise, are linearly correlated.

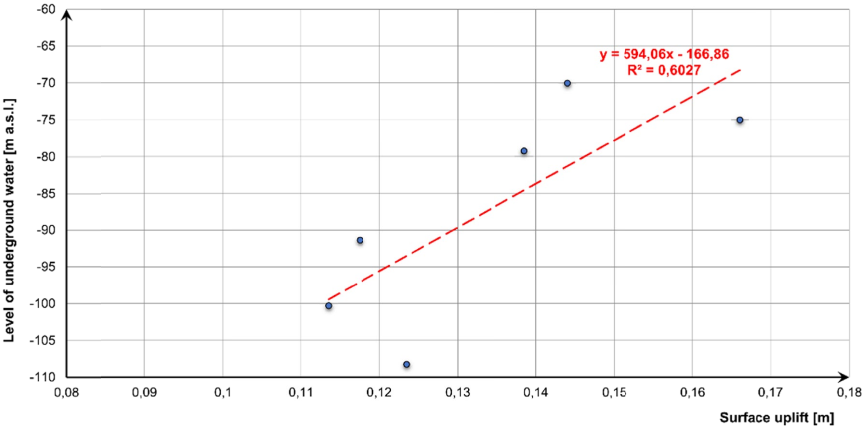

Fig. 8. Change in surface uplift due to the rise in underground water level

5. Numerical modelling

5.1. Model description

Based on the geological and mining conditions in the area of the "Kazimierz-Juliusz" coal mine, a two-dimensional numerical model of the rock mass was constructed using the finite difference method-based code FLAC2D. Due to the lack of primary topographical surface and geological structure data for such a large area at the studied site, the modelled rock mass fragment is represented as a column with the entire extraction depth of the liquidated mine. The model has the following dimensions: width × height = 50 × 700 m. It is divided into 35,000 elements (Fig. 9). Additionally, such a model is optimal due to computational time constraints. Displacement boundary conditions were applied to the lower edge and both sides of the model, while the upper surface remained free.

An essential element of every numerical model is the appropriate selection of mechanical parameters for individual rock layers. Due to the lack of geomechanical research conducted in the coal mine after its closure, a homogeneous rock mass was adopted in the model with weighted average values of the parameters for the rock layers. The rock mass was modelled as an elastic material using a built-in constitutive model (elastic model) available in FLAC2D [88]. The basic values of deformation parameters adopted for the calculations are summarised in TABLE 3.

An important factor influencing surface uplift is the pore water pressure, most often referred to as hydrostatic pressure. The maximum value of pore pressure for given water levels can be easily calculated and assigned to the modelling. Calculations were also carried out for different pore pressure values, reduced from the maximum by 5%, 10%, and 15%.

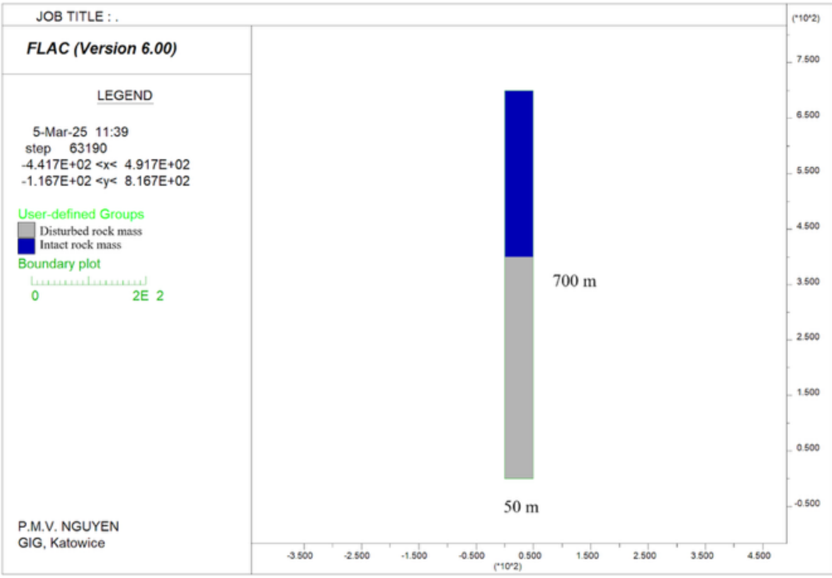

Fig. 9. Model geometry and rock mass distribution in FLAC2D

TABLE 3

Sets of rock mass deformation parameters adopted for numerical calculations

Type of rock mass		Bulk modulus, *K* [GPa]	Shear modulus, *G* [GPa]
Intact rock mass		2.5	1.15
Disturbed rock mass as a result of underground mining	Fractured/jointed rock mass – I	1.35	0.44
	Highly fractured/heavily jointed rock mass – II	0.67	0.14

5.2. Modelling methodology

Based on the described characteristics of groundwater at the studied site, i.e. the water level is raised upstream horizontally. A new phreatic surface develops across the study site that causes the heave of the soil surface as a result of the increase in pore pressure. It is well-known that when pore pressures change due to flow or zone-volume changes, the total stresses are automatically adjusted by the same amount (5):

$$\Delta\sigma_{xx} = \Delta\sigma_{yy} = \Delta\sigma_{zz} = -\alpha\Delta P \tag{5}$$

This means the total stress acting in a zone is the sum of the matrix stress (caused by the forces exerted by the grains of soil or rock matrix) and the fluid pressure, acting in the void spaces. In FLAC2D, the 'adjustment of total stresses' option offers a convenient way to model the effect on heave or subsidence of a soil layer resulting from the raising or lowering of a water table. For such cases, total stresses will be adjusted according to the above equation associated with a change of pore pressures generated in the model, without coupling a fluid flow simulation [88].

Simply, the model was initially calculated to achieve equilibrium for a dry rock mass. The dry density of the material was assigned, and the saturation was set to zero. After that, displacement and velocity vectors were then reset to zero. In the next steps, each water level was assigned by applying pore pressure and a saturation value of 1, and the model was recalculated.

5.3. Model verification

In this study, back analysis was conducted by matching the results of numerical modelling with the measured deformation as outcomes of the monitoring using satellite interferometry described in section 4. The results of the numerical calculations are presented in the form of the maximum vertical displacement values at the upper edge (surface) of the model. TABLE 4 shows the results for all considered calculation variants. It can be observed that the values of surface uplift are proportional to the decrease in deformation parameters of the rock mass and the increase in pore pressure within the rock mass. Fig. 10 shows a comparison of the in-situ deformation and modelling results.

TABLE 4

Maximum vertical displacement of the model upper edge (surface) in [m]

Pore pressure [MPa]		**Levels of underground water, m [a.s.l.]**	**Sets of rock mass deformation parameters for disturbed rock mass**	
			I	**II**
Maximum values	3.26	–108.2	0.139	0.310
	3.34	–100.3	0.146	0.326
	3.42	–91.3	0.153	0.343
	3.54	–79.2	0.164	0.368
	3.58	–74.9	0.168	0.376
	3.63	–70.1	0.173	0.387
5% Reduction	3.10	–108.2	0.125	0.279
	3.17	–100.3	0.131	0.292
	3.25	–91.3	0.138	0.308
	3.36	–79.2	0.148	0.330
	3.40	–74.9	0.151	0.338
	3.45	–70.1	0.156	0.349
10% Reduction	2.93	–108.2	0.111	0.246
	3.01	–100.3	0.116	0.259
	3.08	–91.3	0.123	0.274
	3.19	–79.2	0.132	0.294
	3.22	–74.9	0.134	0.300
	3.27	–70.1	0.138	0.310
15% Reduction	2.77	–108.2	0.097	0.216
	2.84	–100.3	0.102	0.227
	2.91	–91.3	0.107	0.239
	3.01	–79.2	0.115	0.257
	3.04	–74.9	0.117	0.262
	3.09	–70.1	0.121	0.271

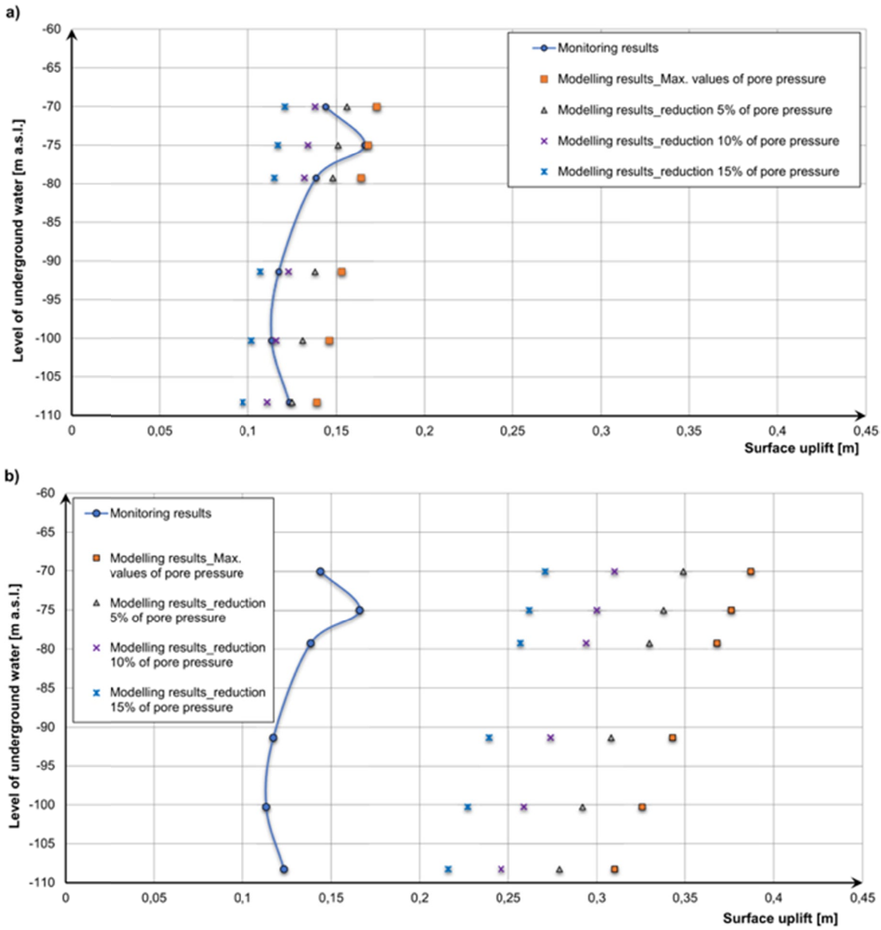

Fig. 10. Comparison of the in-situ deformation and modelling results: a) for set I; b) for set II

It can be noticed that the modelling result values are close to in-situ values in the case of rock mass adopted as set I (fractured/jointed rock mass), while the modelling results are strongly divergent to the monitoring results in the case of set II (highly fractured/heavily jointed rock mass). For set I, it is possible to obtain values of surface uplift close to the monitored values by controlling the pore pressure within a range of 85% to 100% of its maximum value. Moreover, the increased trend function in this case is matched with the monitoring results. Based on this, a data set of the matched variant can be adopted for further numerical modelling in order to predict the evolution of surface deformation with the raised water levels.

5.4. Prediction of surface uplift

Due to the lack of mine water level control, accurately predicting future surface consequences remains challenging. In long-term predictions, it is assumed that the water level will continue to rise and reach the surface. Calculations were carried out for the fractured/jointed rock mass (set I) with the maximum pore pressure assigned for the higher water levels, i.e., sea level, 200 m below ground level, 140 m below ground level, 60 m below ground level and ground level (surface). Fig. 11 presents the surface predictions for these different scenarios of underground water levels. According to these predictions, if water continues to rise, surface uplift can reach up to approx. 60 cm.

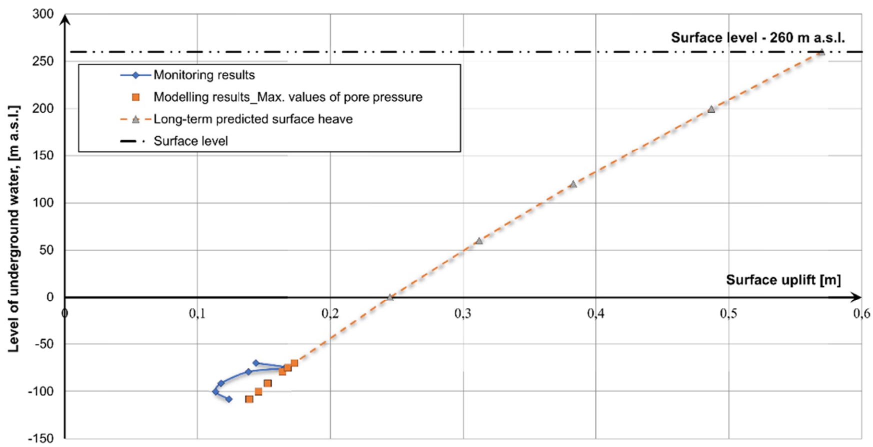

Fig. 11. Long-term predictions of surface uplift

6. Discussion

Surface uplift is rarely observed in post-mining areas due to the natural tendency of the mined mineral body to be filled by the surrounding rock mass, a phenomenon that typically leads to surface subsidence [15,29,30,34,40,89]. However, in the case of flooded mines, the presence of water induces displacements in the rock mass differently due to changes in pore pressure, which in turn alter effective stress and cause mechanical volume changes in the rock mass [9,11,12,80].

The fluid/solid interaction is a complex mechanism that involves the coupling of solid weight, buoyancy, and seepage forces, which recur cyclically over time. Surface uplift caused by raising water level mentioned in the studied site is one type of such an interaction. Despite the simplifications adopted, for modelling the phenomenon has been successfully modelled by controlling the most influential factors: rock mass deformation parameters and pore pressure. The modelling results are unable to capture the 'consolidation' mechanism of the rock mass and water, i.e., upward and downward flow. However, they do show an 'increasing surface uplift' tendency, similar to the monitoring results. It cannot be excluded that rock mass will weaken over time in the waterlogged conditions, while the pore pressure can be increased due to the possible additional surface water supplies (river, rainfall). Therefore the surface uplift is expected to reach a value even higher than the predicted values shown in Fig. 11.

It is equally important to consider the use of the PSInSAR method in future studies [65,66]. By analysing selected persistent surface reflectors, PSInSAR enables deformation detection with millimetre per-year precision and better characterisation of long-term trends. In addition, the method offers the possibility of better separation of local deformations from atmospheric noise and random artefacts, which significantly increases the reliability of the results obtained.

7. Conclusions

Post-mining areas are subject to significant ground deformations, including large-scale land subsidence, surface uplift, and the sudden development of sinkholes, all of which pose considerable risks to infrastructure, the environment, and public safety. Therefore, a thorough understanding and continuous monitoring of these phenomena are essential for mitigating geohazards and ensuring the long-term usability of post-mining areas. To support this effort, a study was conducted to predict surface uplift at the flooded Kazimierz-Juliusz coal mine in Poland. The approach involved numerical modelling using FLAC2D, a finite difference method-based software capable of simulating complex geomechanical behaviour. The development of the model was supported by an extensive dataset obtained through Satellite Interferometric Synthetic Aperture Radar (InSAR) monitoring. Based on the results of the study, the following conclusions can be drawn:

- Monitoring data obtained using Satellite Interferometric Synthetic Aperture Radar (InSAR) indicated the occurrence of surface uplift at the study site, with a maximum displacement of approximately 16 cm recorded between January 2015 and December 2023. The area of greatest deformation was located in the central-western part of the analysed post-mining region.
- Based on the analysis of SBAS-InSAR results, the monitoring method is considered reliable due to the high accuracy of the data obtained. Surface uplift of several centimetres per year was identified, with the method demonstrating an accuracy of approximately 8 mm/year.
- Based on the modelling results, the phenomenon of surface uplift can be modelled by appropriately selecting the rock mass state and pore pressure. For the studied site, the rock mass is considered fractured/jointed due to underground mining throughout the mine's life, while the pore pressure should range from 85% to 100% of its maximum value.
- Due to the lack of information on the hydrogeological conditions of the mechanical properties of rocks in the studied site, such as the porosity and permeability of individual rock layers and pore pressure at different groundwater levels, it is suggested to conduct detailed physico-mechanical and hydrogeological studies. The goal of these studies is to achieve high accuracy and reliability of the results in using 3D modelling.
- Based on the monitoring results, the numerical model has been verified. This is a crucial step in enabling further analysis and ensuring reliable predictions of surface uplift. As a result, the long-term predictions using modelling of surface uplift were presented. Specifically, when the water level reaches sea level, surface uplift is expected to be 24.5 cm, and when the water level reaches the ground level, surface uplift is expected to be 57 cm. These predictions are expected to assist the mine in managing surface land in terms of urban architecture.
- Long-term monitoring of surface uplift and underground water level is essential to fully understand the mechanisms driving such movements and to assess potential risks associated with infrastructure stability and environmental impacts. Its results will also help

confirm and verify the predictions of the numerical modelling. An approach that combines numerical modelling, such as FLAC2D, with monitoring technologies like InSAR can reliably monitor and analyse surface deformation in active mining and post-mining areas. It provides an effective method for predicting the development of surface deformation in later periods.

- To achieve even higher accuracy in future studies, the incorporation of an additional monitoring method, such as the PSInSAR method should be considered.

Funding

This research was funded by the Ministry of Science and Higher Education, Statutory Activity of the Central Mining Institute – National Research Institute in Katowice, Poland No 111820124-120.

References

[1] K. Tajduś, Numerical simulation of underground mining exploitation influence upon terrain surface. Arch. Min. Sci. **58** (3), 605-616 (2013). DOI: https://doi.org/10.2478/amsc-2013-0042

[2] Z. Niedojadło, W. Gruszczyński, The impact of the estimation of the parameters values on the accuracy of predicting the impacts of mining exploitation. Arch. Min. Sci. **60** (1), 173-193 (2015). DOI: https://doi.org/10.1515/amsc-2015-0012

[3] E. Fathi Salmi, M. Nazem, M. Karakus, Numerical analysis of a large landslide induced by coal mining subsidence. Eng. Geol. **217**, 141-152 (2017). DOI: https://doi.org/10.1016/j.enggeo.2016.12.021

[4] W. Gruszczyński, Z. Niedojadło, D. Mrocheń, Influence of model parameter uncerainties on forecasted subsidence. Acta. Geodyn. Geomater. **15** (3), 191 (2018). DOI: https://doi.org/10.13168/agg.2018.0016

[5] A. Guney, M. Gul, Analysis of surface subsidence due to longwall mining under weak geological conditions: Turgut basin of Yataganmugla (Turkey) case study. Int. J. Min. Reclam. Env. **33** (7), 445-461 (2019). DOI: https://doi.org/10.1080/17480930.2018.1443691

[6] J. Białek, M. Wesołowski, R. Mielimąka, P. Sikora, Deformations of mining terrain caused by the partial exploitation in the aspect of measurements and numerical modeling. Sustainability-Basel **12** (12), 5072 (2020). DOI: https://doi.org/10.3390/su12125072

[7] S. Liu, K. Li, W. Shi, Z. Wang, H. Zhang, Z. Li, Analysis of mining subsidence characteristics and deformation prediction considering size parameters and mechanical parameters. Geofluids **10**, 5495509 (2022). DOI: https://doi.org/10.1155/2022/5495509

[8] S. Samsonov, N. d'Oreye, B. Smets, Ground deformation associated with postmining activity at the french–german border revealed by novel InSAR time series method. Int. J. Appl. Earth Obs. **23**, 142-154 (2013). DOI: https://doi.org/10.1016/j.jag.2012.12.008

[9] M. Caro Cuenca, A.J. Hooper, R.F. Hanssen, Surface deformation induced by water influx in the abandoned coal mines in Limburg, the Netherlands observed by satellite radar interferometry. J. Appl. Geophys. **88**, 1-11 (2013). DOI: https://doi. org/10.1016/j.jappgeo.2012.10.003

[10] R. Alvarez, A. Ordonez, E. De Miguel, C. Loredo, Prediction of the flooding of a mining reservoir in NW spain. J. Environ. Manage. **184**, 219-228 (2016). DOI: https://doi.org/10.1016/j.jenvman.2016.09.072

[11] M. Dudek, K. Tajduś, R. Misa, A. Sroka, Predicting of land surface uplift caused by the flooding of underground coal mines – A case study. Int. J. Rock Mech. Min. **132**, 104377 (2020). DOI: https://doi.org/10.1016/ j.ijrmms.2020.104377

[12] J. Zhao, H. Konietzky, M. Herbst, R. Morgenstern, Numerical simulation of flooding induced uplift for abandoned coal mines: simulation schemes and parameter sensitivity. International Journal of Coal Science & Technology **8**, 1238-1249 (2021). DOI: https://doi.org/10.1007/s40789-021-00465-x

[13] I. Sakhno, S. Sakhno, A. Petrenko, O. Barkova, B. Kobylianskyi, Numerical simulation of the surface subsidence evolution caused by the flooding of the longwall goaf during excavation of thin coal seams. IOP Conference Series: Earth and Environmental Science **1254** (1), 012057 (2023). DOI: https://doi.org/10.1088/1755-1315/1254/ 1/012057

[14] G. Modeste, Y. Gunzburger, M, Conin, M. Diallo, Surface displacement induced by underground activites from 2014 to 2019 in the former Lorraine coalfield, northeastern France. Bull. Soc. Geol. Fr. **196** (7), (2025). DOI: https://doi.org/10.1051/bsgf/2025006

[15] H. Kratzsch, Mining Subsidence Engineering. Springer (1983).

[16] E. Popiołek, Ochrona Terenów Górniczych. AGH University of Krakow (2009).

[17] H. Keinhorst, 25 Jahre der Emschergenossemschaft 1900-1925, Selbstverlag der Emschergenossenschaft (1925).

[18] R. Bals, Beitrag zur frage der vorausbrchnung bergbaulicher senkungen. Mitteilungen aus dem Markscheidewesen, **42/43**, 98-111 (1931/32).

[19] S. Knothe, Równanie profilu ostatecznie wykształconej niecki osiadania. Archives of Mining and Metallurgy **1** (1), 22-38 (1953)

[20] S. Knothe, Prognozowanie wpływów eksploatacji górniczej. Silesia (1984).

[21] W. Ehrhardt, A. Sauer, Die vorausberechnung von senkung, schieflage und krümmung über dem abbau in flacher lagerung. Bergb.-Wiss **8**, 415/28 (1961).

[22] A. Sroka, K. Tajduś, R. Misa, Analiza deformacji powierzchni terenu związana z działalnością górnicza przy uwzględnieniu zmieniających się warunków brzegowych. Transactions of the Strata Mechanics Research **16** (3-4), 93-102 (2014).

[23] A. Malinowska, R. Hejmanowski, H. Dai, Ground movements modeling applying adjusted influence function. International Journal of Mining Science and Technology **30** (2), 243-249 (2020). DOI: https://doi.org/10.1016/j.ijmst.2020.01.007

[24] P. Polanin, Application of two parameter groups of the Knothe-Budryk theory in subsidence prediction. Journal of Sustainable Mining **14** (2), 1 (2015). DOI: https://doi.org/10.46873/2300-3960.1230

[25] B. Apanowicz, A. Kowalski, P. Gruchlik, P. Polanin, Examples of the Knothe-Budryk theory parameter determination under complex geological and mining conditions. Mining Science **29**, 19-32 (2022). DOI: https://doi.org/10.37190/msc22903

[26] A. Sroka, S. Hager, R. Misa, K. Tajduś, M. Dudek, The application of Knothe's theory for the planning of mining exploitation under the threat of discontinuous deformation of the surface and for the prediction of ground surface movements with rising water levels in the post-mining phase. Mineral Resources Management **37** (4), 199-218 (2021). DOI: https://doi.org/10.24425/gsm.2021.139737

[27] X.L. Yao, D.J. Reddish, B.N. Whittaker, Non-linear finite element analysis of surface subsidence arising from inclined seam extraction. Int. J. Rock Mech Min. **30** (4), 431-441 (1999). DOI: https://doi.org/10.1016/0148-9062(93)91724-W

[28] W. Keilich, PhD thesis, Numerical Modelling of Mining Subsidence. Upsidence and Valley Closure Using UDEC, University of Wollongong, Wollongong, Australia (2009).

[29] M. Sayyaf, M. Mahdavi, O.R. Barani, S. Feiznia, B. Motamedvaziri, Simulation of land subsidence using finite element method: Rafsanjan plain case study. Nat. Hazards **72** (2), 309-322 (2014). DOI: https://doi.org/10.1007/s11069-013-1010-6

[30] A.M. Suchowerska-Iwanec, J.P. Carter, J.P. Hambleton, Geomechanics of subsidence above single and multi-seam coal mining. Journal of Rock Mechanics and Geotechnical Engineering **8** (3), 304-313 (2016). DOI: https://doi.org/10.1016/j.jrmge.2015.11.007

[31] G. Huang, P.H. Kulatilake, S. Shreedharan, S. Cai, H. Song, 3-D discontinuum numerical modeling of subsidence incorporating ore extraction and backfilling operations in an underground iron mine in China. International Journal of Mining Science and Technology **27** (2), 191-201 (2017). DOI: https://doi.org/10.1016/j.ijmst.2017.01.015

[32] R. Das, P.K. Singh, A. Kainthola, S. Panthee, T.N. Singh, Numerical analysis of surface subsidence in asymmetric parallel highway tunnels. Journal of Rock Mechanics and Geotechnical Engineering **9** (1), 170-179 (2017). DOI: https://doi.org/10.1016/j.jrmge.2016.11.009

[33] P. Hamdi, D. Stead, D. Elmo, J. Toyra, Use of an integrated finite/discrete element method-discrete fracture network approach to characterize surface subsidence associated with sub-level caving. Int. J. Rock Mech. Min. **103**, 55-67 (2018). DOI: https://doi.org/10.1016/j.ijrmms.2018.01.021

[34] W. Cao, X. Wang, P. Li, D. Zhang, C. Sun, D. Qin, Wide strip backfill mining for surface subsidence control and its application in critical mining conditions of a coal mine. Sustainability-Basel **10** (3) (2018). DOI: https://doi.org/10.3390/su10030700

[35] G.Z. Voyiadjis, Y. Zhou, Time-dependent modeling of subsidence due to drainage in bounding shales: Application to a depleted gas field in Louisiana. J. Petrol. Sci. Eng. **166**, 175-187 (2018). DOI: https://doi.org/10.1016/j.petrol.2018.03.032

[36] X. Li, D. Wang, C. Li, Z. Liu, Numerical simulation of surface subsidence and backfill material movement induced by underground mining. Advances in Civil Engineering **2019** (1), 2724370 (2019). DOI: https://doi.org/10.1155/2019/2724370

[37] Y. Shi, M. Zhao, J. Hao, Study on numerical models in predicting surface deformation caused by underground coal mining. Geotechnical and Geological Engineering **39**, 4457-4473 (2021). DOI: https://doi.org/10.1007/s10706-021-01775-2

[38] X. Zhao, W. Yu, Y. Zhao, S. Fu, Numerical estimation of shaft stability and surface deformation induced by underground mining transferred from open-pit mining in Jinfeng gold mine. Minerals-Basel **13** (2), (2023). DOI: https://doi.org/10.3390/min13020196

[39] Y. Guo, L. Luo, R. Ma, S. Li, W. Zhang, C. Wang, Study on surface deformation and movement caused by deep continuous mining of steeply inclined ore bodies. Sustainability-Basel **15** (15), 11815 (2023). DOI: https://doi.org/10.3390/su151511815

[40] Z. Li, K. Hou, T. Li, J. Tang, G. Lu, Numerical Simulation of Surface Subsidence and Fracture Evolution Caused by Pulang Copper Mine Mining. Appl. Sci.-Basel **14** (6), 2416 (2024). DOI: https://doi.org/10.3390/app14062416

[41] M. Kwaśniewski, J. Wang, Analiza numeryczna deformacji górotworu wywołanych eksploatacją górniczą. Conference proceedings School of Underground Mining (1996).

[42] L. Florkowska, Modelowanie numeryczne wpływu górniczych deformacji podłoża na grupę budynków w zwartej zabudowie miejskiej. AGH Journal of Mining and Geoengineering **33** (1) (2009).

[43] K. Tajduś, PhD thesis, Określanie wartości parametrów odkształceniowych górotworu uwarstwionego w rejonie wpływów eksploatacji górniczej. AGH University of Krakow, Krakow, Poland (2008).

[44] K. Tajduś, New method for determining the elastic parameters of rock mass layers in the region of underground mining influence. Int. J. Rock Mech. Min. **46** (8), 1296-1305 (2009). DOI: https://doi.org/10.1016/j.ijrmms.2009.04.006

[45] K. Tajduś, A. Sroka, A. Tajduś, A. Preusse, Three dimensional modelling of a surface displacements as a result of an underground longwall panel extraction. 29th International Conference on Ground Control in Mining, 105-110 (2010).

[46] K. Tajduś, Numerical modelling of the mining induced horizontal displacement. Studia Geotechnica et Mechanica, **37** (4), 65-73 (2016). DOI: https://doi.org/10.1515/sgem-2015-0046

[47] M. Wesołowski, J. Białek, P. Kołodziejczyk, F. Plewa, Modelowanie wpływów eksploatacji górniczej przy wykorzystaniu modeli numerycznych. Silesian University of Technology (2010).

[48] M. Wesołowski, Zastosowanie liniowego ośrodka transwersalnie izotropowego do modelowania deformacji terenu górniczego. Silesian University of Technology (2013).

[49] M. Dudek, K. Tajduś, FEM for prediction of surface deformations induced by flooding of steeply inclined mining seams. Geomechanics for Energy and the Environment **28**, 100254 (2021). DOI: https://doi.org/10.1016/j.gete.2021.100254

[50] M. Dudek, D. Mrocheń, A. Sroka, K. Tajduś, Integrating the finite element method with Python scripting to assess mining impacts on surface deformations. App. Sci.-Basel **14** (17), 7797 (2024). DOI: https://doi.org/10.3390/app14177797

[51] J. Zhao, H. Konietzky, M. Herbst, R. Morgenstern, Numerical simulation of flooding induced uplift for abandoned coal mines: simulation schemes and parameter sensitivity. Int. J. Coal Sci. Technol. **8** (6), 1238-1249 (2021). DOI: https://doi.org/10.1007/s40789-021-00465-x

[52] J. Zhao, H. Konietzky, Numerical analysis and prediction of ground surface movement induced by coal mining and subsequent ground flooding. Int. J. Coal Geol. **229**, 103565 (2020). DOI: https://doi.org/10.1016/j.coal.2020.103565

[53] F. Todd, C. McDermott, AF. Harris, A. Bond, S. Gilfillan, Coupled hydraulic and mechanical model of surface uplift due to mine water rebound: Implications for mine water heating and cooling schemes. Scott. J. Geol. (2019). DOI: https://doi.org/10.1144/sjg2018-028

[54] X. Yin, J. Chai, W. Deng, Z. Yang G. Tian, C. Gao, Pointwise Modelling and Prediction for Ground Surface Uplifts in Abandoned Coal Mines from InSAR Observations. Remote Sens.-Basel **15** (9), 2337 (2023). DOI: https://doi.org/10.3390/rs15092337

[55] P. Sopata, V. Sokoła-Szewioła, Qualitative relationship of seismic activity with vertical displacement of terrain after mine closure with the use of DInSAR technology. Geoinf. Pol. **21**, 83-93 (2022). DOI: https://doi.org/10.4467/21995923GP.22.006.17084

[56] Postminquake Consortium, PostMinQuake RFCS Research Project (2020-2023). https://postminquake.eu/dpid-library, accessed: 09.12.2024

[57] H.A. Zebker, R.M. Goldstein, Topographic mapping from interferometric synthetic aperture radar observations. J. Geophys. Res-Sol. Ea. **91** (B5), 4993-4999 (1986). DOI: https://doi.org/10.1029/jb091ib05p04993

[58] A. Ferretti, Satellite InSAR Data: Reservoir Monitoring from Space (EET 9). EAGE Publications bv (2014). DOI: https://doi.org/10.3997/9789462820036

[59] R.F. Hanssen, PhD thesis, Radar interferometry: Data interpretation and error analysis. Technische Universiteit Delft, Faculty of Civil Engineering and Geosciences, Delft, Netherlands (2001).

[60] A. Ferretti, A. Monti-Guarnieri, C. Prati, F. Rocca, D. Massonnet, InSAR Principles: Guidelines for SAR Interferometry Processing and Interpretation. ESA Publications (2007).

[61] C. Chen, H. Zebker, Network approaches to two-dimensional phase unwrapping: intractability and two new algorithms. Journal of the Optical Society of America **17**, 401-414 (2000). DOI: https://doi.org/10.1364/josaa.17.000401

[62] C. Chen, H. Zebker, Two-dimensional phase unwrapping with use of statistical models for cost functions in nonlinear optimization. Journal of the Optical Society of America **18**, 338-351 (2001). DOI: https://doi.org/10.1364/josaa.18.000338

[63] C. Chen, H. Zebker, Phase unwrapping for large SAR interferograms: statistical segmentation and generalized network models. IEEE T. Geosci. Remote **40** (8), 1709-1719 (2002). DOI: https://doi.org/10.1109/tgrs.2002.802453

[64] C. Carnec, D. Massonet, C. King, Two examples of the use of SAR interferometry on displacement fields of small spatial extent. Geophys. Res. Lett. **23** (24), 3579-3582 (1996). DOI: https://doi.org/10.1029/96gl03042

[65] A. Ferretti, C. Prati, F. Rocca, Nonlinear subsidence rate estimation using permanent scatterers in differential SAR interferometry. IEEE T. Geosci. Remote **38** (5), 2202-2212 (2000). DOI: https://doi.org/10.1109/36.868878

[66] A. Ferretti, C. Prati, F. Rocca, Permanent scatterers InSAR interferometry. IEEE T. Geosci. Remote **39** (1), 8-20 (2001). DOI: https://doi.org/10.1109/36.898661

[67] P. Berardino, G. Fornaro, R. Lanari, E. Sansosti, A new algorithm for surface deformation monitoring based on small baseline differential SAR interferograms. IEEE T. Geosci. Remote **40** (11), 2375-2383 (2002). DOI: https://doi.org/10.1109/tgrs.2002.803792

[68] A. Hooper, H. Zebker, P. Segall, B. Kampes, A new method for measuring deformation on volcanoes and other natural terrains using InSAR persistent scatterers. Geophys. Res. Lett. **31** (23) (2004). DOI: https://doi.org/10.1029/2004GL021737

[69] C. Yang, Q. Zhang, C. Zhao, L. Ji, W. Zhu, Monitoring mine collapse by D-InSAR. Mining Science and Technology (China) **20** (5), 696-700 (2010). DOI: https://doi.org/10.1016/s1674-5264(09)60265-9

[70] N.B. Bechor, H.A. Zebker, Measuring two-dimensional movements using a single InSAR pair. Geophys. Res. Lett. **33** (16) (2006). DOI: https://doi.org/10.1029/2006gl026883

[71] O. Beladam, T. Balz, B. Mohamadi, M. Abdalhak, Using PS-InSAR with Sentinel-1 images for deformation monitoring in northeast Algeria. Geosciences **9** (7), 315 (2019). DOI: https://doi.org/10.3390/geosciences9070315

[72] T. Strozzi, R. Caduff, N. Jones, C. Barboux, R. Delaloye, X. Bodin, A. Kaab, E. Matzler, L. Schrott, Monitoring rock glacier kinematics with satellite synthetic aperture radar. Remote Sens.-Basel **12** (3), 559 (2020). DOI: https://doi.org/10.3390/rs12030559

[73] K.R. Anderson, M.P. Poland, Bayesian estimation of magma supply, storage, and eruption rates using a multiphysical volcano model: Kīlauea Volcano, 2000-2012. Earth Planet. Sc. Lett. **447**, 161-171 (2016). DOI: https://doi.org/10.1016/j.epsl.2016.04.029

[74] S. Tung, T. Masterlark, Coseismic slip distribution of the 2015 Mw7.8 Gorkha, Nepal, earthquake from joint inversion of GPS and InSAR data for slip within a 3-D heterogeneous Domain. J. Geophys. Res-Sol. Ea. **121** (5), 3479-3503 (2016). DOI: https://doi.org/10.1002/2015jb012497

[75] A.H.-M. Ng, L. Ge, Y. Yan, X. Li, H.-C. Chang, K. Zhang, C. Rizos, Mapping accumulated mine subsidence using small stack of SAR differential interferograms in the southern coalfield of New South Wales. Australia, Eng. Geol. **115** (1), 1-15 (2010). DOI: https://doi.org/10.1016/j.enggeo.2010.07.004

[76] Y. Chen, Y. Tong, K. Tan, Coal mining deformation monitoring using SBAS-InSAR and offset tracking: A case study of Yu County, China. IEEE J. Sel. Top. Appl. **13**, 6077-6087 (2020). DOI: https://doi.org/10.1109/jstars.2020.3028083

[77] B. Apanowicz, Use of InSAR in linear discontinuous ground deformation generation analysis: Case study of a mine in Poland. Journal of Sustainable Mining **21** (1), 45-53 (2022). DOI: https://doi.org/10.46873/2300-3960.1346

[78] Y. Gueguen, B. Deffontaines, B. Fruneau, M. Al Heib, M. de Michele, D. Raucoules, Y. Guise, J. Planchenault, Monitoring residual mining subsidence of Nord/Pas-de-Calais coal basin from differential and persistent scatterer interferometry (northern France). J. Appl. Geophys. **69** (1), 24-34 (2009). DOI: https://doi.org/10.1016/j.jappgeo.2009.02.008

[79] A. Vervoort, P.-Y. Declercq, Surface movement above old coal longwalls after mine closure. International Journal of Mining Science and Technology **27** (3), 481-490 (2017). DOI: https://doi.org/10.1016/j.ijmst.2017.03.007

[80] A. Vervoort, P.-Y. Declercq, Upward surface movement above deep coal mines after closure and flooding of underground workings. International Journal of Mining Science and Technology **28** (1), 53-59 (2018). DOI: https://doi.org/10.1016/j.ijmst.2017.11.008

[81] P.-Y. Declercq, M. Dusar, E. Pirard, J. Verbeurgt, A. Choopani, X. Devleeschouwer, Post mining ground deformations transition related to coal mines closure in the Campine coal basin, Belgium, evidenced by three decades of MT-InSAR data. Remote Sens.-Basel **15** (3), 725 (2023). DOI: https://doi.org/10.3390/rs15030725

[82] D. Sandwell, R. Mellors, X. Tong, M. Wei, P. Wessel, Open radar interferometry software for mapping surface deformation. Eos, Transactions American Geophysical Union **92** (28), 234-234 (2011). DOI: https://doi.org/10.1029/2011eo280002

[83] T. Farr, P.A. Rosen, E. Caro, R. Crippen, R. Duren, S. Hensley, M. Kobrick, M. Paller, E. Rodriguez, L. Roth, D. Seal, S. Shaffer, J. Shimada, M. Umland, The shuttle radar topography mission. Rev. Geophys. **45** (2), RG2004 (2007). DOI: https://doi.org/10.1029/2005rg000183

[84] C. Yu, N.T. Penna, Z. Li, Generation of real-time mode high-resolution water vapor fields from GPS observations. J. Geophys. Res-Atmos. **122** (3), 2008-2025 (2017). DOI: https://doi.org/10.1002/2016jd025753

[85] C. Yu, Z. Li, N.T. Penna, Interferometric synthetic aperture radar atmospheric correction using a gps-based iterative tropospheric decomposition model. Remote Sens. Environ. **204**, 109-121 (2018). DOI: https://doi.org/10.1016/j.rse.2017.10. 038

[86] C. Yu, Z. Li, N.T. Penna, P. Crippa, Generic atmospheric correction model for interferometric synthetic aperture radar observations. J. Geophys. Res-Sol. Ea. **123** (10), 9202-9222 (2018). DOI: https://doi.org/10.1029/2017jb015305

[87] P. Wessel, J.F. Luis, L. Uieda, R. Scharroo, F. Wobbe, W.H.F. Smith, D. Tian, The generic mapping tools version 6. Geochem. Geophy. Geosy. **20** (11), 5556-5564 (2019). DOI: https://doi.org/10.1029/2019gc008515

[88] Itasca Consulting Group Inc.: FLAC2D, Version 6.0. Software available at www.itascacg.com, (2008).

[89] B.N. Whittaker, D.J. Reddish, Subsidence Occurrence, Prediction and Control, Elsevier Science (1989).